Construction and experimental validation of ferroptosis-related competing endogenous RNA networks in hepatocellular carcinoma based on WGCNA

Ting Guo
Sichuan University, Sichuan University
Kun He
Xijing Hospital, Airforce Military Medical University
Weigang Chen
Xijing Hospital, Airforce Military Medical University
Mengwei Xu
Xijing Hospital, Airforce Military Medical University
Jingjing Sun
Xijing Hospital, Airforce Military Medical University
Yong Chen
Xijing Hospital, Airforce Military Medical University
Zelong Yang (youngderl@hotmail.com)
Xijing Hospital, Airforce Military Medical University

Article

Keywords: Hepatocellular Carcinoma, Competing endogenous RNA, Ferroptosis, TCGA, WGCNA, miR-23b-3p

Posted Date: July 26th, 2022

DOI: https://doi.org/10.21203/rs.3.rs-1869613/v1

Abstract

The ferroptosis-related competing endogenous RNAs (ceRNA) network in hepatocellular carcinoma (HCC) has not been fully explored. In this study, RNA sequence data of HCC and clinic data were downloaded from The Cancer Genome Atlas (TCGA) database. Through the pre-set three gene sets of autophagy, pyroptosis, and ferroptosis, each sample was scored by single-sample Gene Set Enrichment Analysis (ssGSEA), and ferroptosis was associated with overall survival. We used Weighted Gene Co-Expression Network Analysis (WGCNA) analysis to modularize long non-coding RNA (lncRNA), microRNA (miRNA), and messenger RNA (mRNA). The most ferroptosis related modules were identified by correlation analysis. Enrichment analysis showed the genes were significantly enriched in ferroptosis-related functions and pathways. The ceRNA network was constructed by the prediction from online tools. We randomly selected one axis for laboratory verification, the DNAJC27-AS1/miR-23b-3p/PPIF axis. Functionally, DNAJC27-AS1 and PPIF could negatively regulate the level of ferroptosis in HCC cells, while miR-23b-3p played positively. Mechanistically, miR-23b-3p can directly bind to DNAJC27-AS1 and PPIF, respectively. DNAJC27-AS1 and PPIF can regulate mutually through sponging miR-23b-3p and act as potential ferroptosis regulators. Taken together, we provided a reliable ferroptosis-related ceRNA network and preliminarily verified it. This study may offer new insights for future research on ferroptosis in HCC.

Introduction

Hepatocellular carcinoma is the predominant histological form of primary liver cancer, with a high incidence and mortality worldwide (1). Hepatitis B or C virus infection, alcohol, smoking, and nonalcoholic fatty liver disease are the most common risk factors for HCC development (2). There are various treatment modalities for HCC nowadays, including surgery, transplantation, ablative and systemic therapy, and targeted treatment. Although more and more mechanisms behind the development and progression of HCC have been unearthed, the treatment efficacy is still unsatisfactory; the 5-year survival rate for HCC patients is only 18% (3). The need for further expanding the therapeutic efficacy of HCC remains unmet.

The induction of cell death is a promising approach for cancer treatment (4). Different forms of regulated cell death (RCD) have different effects on carcinogenesis and development of HCC, and most RCDs play a role as a double-edged sword (5). However, most researchers have focused on apoptosis (6). In 2012, Dixon et al. firstly described a new type of RCD, ferroptosis, which is morphologically and biochemically different from apoptosis (7). Ferroptosis can be induced by Erastin, a selective cell death inducer in cancer cells with genetically mutated RAS (8). Erastin was also a reasonable retarder for xCT, a cystine-glutamate antiporter encoded by the SLC7A11 gene, which is indispensable for importing extracellular cystine into tissue cells. Cystine is the primary material for producing glutathione (GSH), which could reduce the intracellular lipid peroxidation level by regulating glutathione peroxidase 4 (GPX4). Dysfunction in GPX4 and its related genes may lead to superoxide accumulation, mitochondrial damage, and ferroptosis (9). Many factors, such as iron overload (10), and p53 protein (11), could induce ferroptosis. So ferroptosis is a polygenic RCD that exists in oxidative and iron-dependent forms, which are

involved in many liver diseases, such as hepatic ischemia-reperfusion injury, liver fibrosis, nonalcoholic steatosis, and liver failure (12). A recent study demonstrated that liver cancer cells could be inhibited by inducing ferroptosis (13). In addition, after the use of sorafenib, a kind of systemic agent approved for HCC, most advanced HCC patients are resistant to sorafenib, and some studies have advocated that targeting ferroptosis can ameliorate sorafenib resistance (14, 15). So, an improved understanding of ferroptotic regulatory networks in HCC is necessary.

Competing endogenous RNA is a complex post-transcriptional regulatory mode that was usually described as lncRNA and mRNA competing with miRNA through response elements (16). LncRNA with complementary sequences to their target miRNA can decrease the ability of miRNA to bind with mRNA, thus upregulating the expression of miRNA target genes. The classical lncRNA-miRNA-mRNA ceRNA network has been discovered in the progression and pathogenesis of various cancers by regulating mRNA expression and protein levels, such as liver cancer (17) and gallbladder cancer (18), and so forth. A recent study indicated that the lncRNA-miRNA-mRNA network could be a prognostic marker for pancreatic adenocarcinoma (19) and a therapeutic target for colorectal cancer (20). Interestingly, non-coding RNA has been found to regulate ferroptosis in cancers (21). For example, lncRNA NEAT1 was reported to promote MIOX expression by competitively binding to miR-362-3p and decreasing intracellular NADPH and GSH levels, thereby enhancing Erastin- and RSL3-induced ferroptosis in HCC cells (22). The cytosolic P53RRA-G3BP1 interaction can transpose p53 to the nucleus, which leads to cell-cycle arrest, apoptosis, and ferroptosis (23). However, the association between ceRNA and ferroptosis in HCC has not been fully unveiled.

This study obtained HCC patients' clinical and RNA expression data from the TCGA database. Through the ssGSEA scoring and the WGCNA analysis, we identified the ferroptosis-associated mRNAs, lncRNAs, and miRNAs. Next, using multiple online tools, we predicted the target lncRNAs and mRNAs of the ferroptosis-associated miRNAs. Finally, we constructed ceRNA networks based on the hub lncRNAs and validated one ceRNA axis of the networks through various lab experiments.

Results

1. The ssGSEA score of ferroptosis is strongly associated with the survival of HCC patients.

The visual flow-process diagram of this study is presented in **Figure 1**. According to the expression levels of genes related to pyroptosis, autophagy, and ferroptosis in each sample, ssGSEA scores were performed. The heat map and boxplot of the enrichment scores are shown in **Figure 2A** and **2B**. Next, we analyzed the differences in the enrichment scores between cancerous and adjacent non-cancerous tissues. As a result, ferroptosis-related enrichment scores were not different between the two tissues, whereas pyroptosis and autophagy-related scores were different (**Figure 2C**). However, through Kaplan-Meier survival analysis, as well as univariate COX regression, we found that only ferroptosis-related scores were associated with overall survival (HR=216, 95% CI [3.03-15400], p=0.0135), and patients with higher ferroptosis-related scores had a worse prognosis (p=0.0183). Even in multivariate COX regression,

ferroptosis-related scores correlated with survival (HR=322, *p*=0.0655) (**Figure 2D-2H**). The results of the ssGSEA score are presented in **Supplementary Material 1.**

2. Identification of genes closely associated with ssGSEA scores of ferroptosis via WGCNA

Here, according to the expression levels of mRNA, lncRNA, and miRNA, the co-expression analysis was carried out with the WGCNA package, and the soft thresholding power β was first calculated as 6 when WGCNA analyzed the mRNA data. Then the scale independence reached 0.805, and relatively high-average connectivity was guaranteed (**Figure 3A**). After constructing a clustering tree according to the correlation between the expression of mRNA genes and dividing them into different modules, the correlation analysis of gene expression in each module and ferroptosis-related ssGSEA scores were conducted. It was found that the genes in the royal blue (R=0.29, p<0.001) and the salmon (R=0.23, p<0.001) modules had the strongest positive correlation with the enrichment scores, and the grey (R=-0.18, p<0.001) module had the strongest negative correlation with the enrichment scores (**Figure 3B, 3C**). In the WGCNA analysis of lncRNAs, the genes in the dark green (R=0.18, p<0.001) and the dark red (R=0.16, p=0.001) modules had the strongest positive correlation with the enrichment scores, and the genes in the blue (R=-0.2, p<0.001) module had the strongest negative correlation with the enrichment scores (**Figure 3D-3F**). The miRNAs in the turquoise module (R=0.18, p<0.001) had the strongest positive correlation with the enrichment scores, and the miRNAs in the red module (R=-0.12, p=0.011) had the strongest negative correlation with the enrichment scores (**Figure 3G-3I**).

3. Differential analysis, correlation analysis, and ceRNA network construction

After using miRMap, miRanda, miRDB, TargetScan and miTarBase to predict the miRNAs and mRNAs in the modules most related to ferroptosis, a total of 652 pairs of miRNAs that are positively correlated with ferroptosis and mRNAs that are negatively correlated with ferroptosis were obtained (at least four databases predicted). Thirty-three pairs of miRNAs were negatively associated with death, and mRNAs were positively associated with ferroptosis (predicted by at least two databases). According to the miRcode and starBase databases, we predicted the binding of miRNAs to lncRNAs. Eleven miRNAs are positively correlated with ferroptosis and lncRNAs negatively correlated with ferroptosis (predicted by at least two databases), and 13 pairs of miRNAs are negatively correlated with ferroptosis and lncRNAs that are positively correlated with ferroptosis (predicted by miRcode). After combining the two above prediction results, the ceRNA network centered on miRNAs positively associated with ferroptosis is presented in **Figure 4A**, and the ceRNA network centered on miRNAs negatively correlated with ferroptosis is shown in **Figure 4B**. All mRNAs, lncRNAs, and miRNAs in the two networks were analyzed for differences and correlations, which are presented in **Figure S1A-S1C** and **Figure S2**. Venn diagram for prediction of mRNA-miRNA interactions using multiple databases is shown in **Figure S1D**. Details of mRNA-miRNA interaction prediction and lncRNA-miRNA interaction prediction are provided in **Supplementary Material 2** and **Supplementary Material 3**.

4. Functional enrichment analysis of genes in interested modules

Go enrichment and KEGG enrichment analysis were conducted on the interested modules' genes. In the biological process, the genes in the grey module were representatively enriched in ferroptosis-related processes, such as GO:0019216 (Regulation of lipid metabolic process), GO:0016042 (Lipid catabolic process), GO:0055088 (Lipid homeostasis), GO:0071248 (Cellular response to metal ion). In the cellular component, the genes in the grey module were mainly enriched in GO:0060205 (Cytoplasmic vesicle lumen), GO:0031983 (Vesicle lumen), GO:0005759 (Mitochondrial matrix), and GO:0005788 (Endoplasmic reticulum lumen). In the molecular function, the genes in the grey module were mainly enriched in GO:0016614 (Oxidoreductase activity), GO:0050662 (Coenzyme binding), GO:0048018 (Receptor ligand activity), and GO:0004857 (Enzyme inhibitor activity). KEGG enrichment analysis showed that the genes in the grey module were mainly enriched in hsa03320 (PPAR signaling pathway), hsa00480 (Glutathione metabolism), hsa04657 (IL-17 signaling pathway), hsa04068 (FoxO signaling pathway) (**Figure S3A-S3D**). The genes of royal blue and salmon color modules were merged and then analyzed. They were mainly enriched in GO:0022900 (Electron transport chain), GO:0042775 (Mitochondrial ATP synthesis coupled electron transport), GO:0005852 (Eukaryotic translation initiation factor 3 complex), GO:0016605 (PML body), GO:0009055 (Electron transfer activity), GO:0004032 (Alditol: NADP+ 1-oxidoreductase activity), GO:0016655 (oxidoreductase activity), etc. (**Figure S3E**). Detailed results can be found in **Supplementary Material 4**.

5. Verification of DNAJC27-AS1/ miR-23b-3p/PPIF as a ceRNA axis

To verify the credibility of this ferroptosis-related ceRNA network, we randomly selected two ceRNA axis in the two networks for laboratory validation, namely the DNAJC27-AS1/miR-23b-3p/PPIF axis and AC004988.1/miR-508-3p/C8orf33 axis. However, through qPCR verification, it was found that among the four human HCC cell lines, the differences in the expression levels of DNAJC27-AS1 and miR-23b-3p were more apparent and operable, so we decided to choose DNAJC27-AS1/miR-23b-3p/PPIF axis to verification (**Figure S4A-S4C**). We first constructed the overexpression plasmids and siRNA of DNAJC27-AS1, miR-23b-3p, and PPIF and verified the effect after transfection (**Figure S4D-S4G**, **Figure 5A**, **5E-5F**). After overexpressing or interfering with the expression of miR-23b-3p, the expressions of DNAJC27-AS1 and PPIF were also regulated oppositely. After interfering with DNAJC27-AS1, the expression of PPIF also decreased simultaneously, and after overexpression of PPIF, the expression of DNAJC27-AS1 also increased accordingly (**Figure 5A-5F**).

The accurate interaction site of miR-23b-3p and PPIF was predicted using the Targetscan website tool. The dual luciferase reporter assay also showed that miR-23b-3p directly binds to and modulates PPIF but not the mutant (**Figure 5G**). The accurate interaction site of miR-23b-3p and DNAJC27−AS1 was predicted using BiBiServ2-RNAhybrid, and the dual luciferase reporter assay demonstrated that miR-23b-3p directly binds to and modulates DNAJC27−AS1, but not the DNAJC27−AS1 mutant (**Figure 5H**).

6. DNAJC27-AS1/miR-23b-3p/PPIF axis regulates ferroptosis in HCC cells

Knockdown of DNAJC27−AS1 expression resulted in a reduction in GSH in BEL7402 cells, which was rescued by the use of Fer-1, and the GSH-protective effect of Fer-1 could be abolished by overexpression

of PPIF or miR-23b-3p inhibitor. miR-23b-3p mimics can also reduce GSH levels but can be rescued by overexpression of PPIF (**Figure 6A**). Similarly, Erastin reduced the content of GSH in HepG2 cells, which the DNAJC27–AS1 overexpression plasmid can restore. But the effect of DNAJC27–AS1 to increase GSH can be offset by PPIF downregulation or miR-23b-3p upregulation. miR-23b-3p inhibitor increased GSH, which Erastin decreased, but this phenomenon can be rescued by PPIF interference (**Figure 6B**). The results of CCK8 and ROS detection kept consistent with the results of GSH (**Figure 6C-6F**). Through the results in **Figure 7A**, we found that DNAJC27–AS1 and PPIF can rescue the reduction of mitochondrial membrane potential in HCC cells caused by Erastin. At the same time, miR-23b-3p can promote mitochondrial membrane potential by inhibiting DNAJC27–AS1 and PPIF expression. In particular, it was verified by three ferroptosis markers, GPX4, SLC7A11, and TP53 (**Figure 7B**).

Discussion

HCC is the second leading cause of cancer-related deaths around the world, and it is refractory to nearly all available anti-cancer therapies so far (24). Sorafenib is the first drug approved by the Food and Drug Administration for the systemic treatment of advanced HCC. Sorafenib can significantly prolong the survival of HCC patients by 2.3 to 2.8 months but is susceptible to drug resistance, leading to a poor prognosis (25). The cytotoxic effect of sorafenib could be attributed to the induction of oxidative stress and ferroptosis (26). Targeting ferroptosis could address sorafenib resistance and enhance its therapeutic efficacy; investigators have reported increasing pathways and genes related to ferroptosis and sorafenib resistance in HCC, such as TP53 mutant (27), Rb protein (28), p62-Keap1-Nrf2 pathway (29). In this study, we preselected three gene sets associated with autophagy, pyroptosis, and ferroptosis, respectively. After the ssGSEA scoring, it was found that although the scores of the ferroptosis gene set were not different between cancer and adjacent tissues, only the score of the ferroptosis was associated with the overall survival of patients, so the ferroptosis-related gene set was selected as the basis to construct ceRNA network.

The ceRNA mechanism, a post-transcriptional regulation model, was proposed in 2011, which mainly describes the competitive binding between sponge RNA and miRNA target genes and the regulation of miRNA target gene activity (30). Although the functions of most lncRNAs are still unclear, they are closely related to the occurrence and development of HCC. Accumulating evidence suggests that lncRNAs may regulate HCC progression by ceRNA mechanisms, and some lncRNAs can mediate the same phenotype by interacting with different miRNAs in the HCC pathophysiological process. For example, the lncRNA MALAT1 promotes HCC migration and invasion by three ceRNA axis, namely MALAT1/miR-30a-5p/Vimentin, MALAT1/miR-204/SIRT1, MALAT1/ miR-143-3p/ZEB1 axis (31–33). Certainly, lncRNAs can also mediate different phenotypes by interacting with different miRNAs. HULC is one of the most upregulated lncRNAs in HCC; it affects the expression of CREB by interacting with miR-372, thereby enhancing chromatin accessibility and transcription (34); it also regulates the epithelial-mesenchymal transition of HCC cells via HULC/miR-200a-3p/ZEB1 ceRNA axis (35). The HULC/USP22/Sirt1 axis, a protective autophagy pathway, was verified to weaken the chemosensitivity of HCC cells toward chemotherapeutic agents (36). So far, there is no report on the ceRNA mechanism of ferroptosis in liver

cancer cells and other tumor types, except only one ferroptosis-related ceRNA network in lung cancer, was reported based on bioinformatic analysis (37). Through WGCNA analysis, we found some modules that were most related to ferroptosis, used a variety of prediction software to make predictions centered on miRNAs, and constructed a ferroptosis-related ceRNA network in HCC. To improve the prediction accuracy, we adopted strict screening criteria. When multiple prediction software showed the exact interaction between two RNAs, we considered incorporating this interaction into the network construction.

Next, we verified one axis in our constructed ceRNA network, the DNAJC27 – AS1/ miR-23b-3p /PPIF axis. The gene encoding DNAJC27-AS1 is located in the middle of the long arm at chromosome 2; there are very few studies on the function and mechanism of DNAJC27-AS1. Only one study in the bioinformatics analysis of open-angle glaucoma found that the bioprocess of DNAJC27-AS1 is enriched in regulating some cancers and ferroptosis-related pathways such as MAPK and Wnt pathways (38). In our study, we identified it could negatively regulate the level of ferroptosis in hepatoma cells, and overexpression of DNAJC27-AS1 could reduce Erastin-mediated cell death and ROS levels while rescuing the Erastin-mediated reduction in GSH levels. The mechanism lies in DNAJC27-AS1 directly interacting with miR-23b-3p, then regulating miR-23b-3p and its target gene PPIF, thereby affecting the level of ferroptosis. This is a typical ceRNA competition mechanism in which the core miRNA, miR-23b-3p, was reported to be the oncogene of HCC, and HCC patients with elevated miR-23b-3p expression had a worse prognosis (39). But there is no report on the correlation between miR-23b-3p and ferroptosis in HCC. Some researchers found that after sorafenib treatment, the level of circulating miR-23b-3p in the serum of HCC patients was significantly increased (40); in our study, miR-23b-3p was positively associated with ferroptosis levels, and patients with elevated ferroptosis had a shorter OS. As for ceRNA that miR-23b-3p participates in, it has been reported that SNGH16 and EGF1 regulate autophagy and sorafenib resistance in HCC cells through a ceRNA mechanism by regulating miR-23b-3p (41). In addition, LncRNA HOTAIR increased the expression of ZEB1 by sponging miR-23b-3p, thereby promoting HCC invasion and metastasis (42). In our study, we also found that miR-23b-3p regulates the ferroptosis of hepatoma cells in a ceRNA manner by interacting with DNAJC27-AS1 and PPIF, respectively. This indicates that miR-23b-3p regulates different phenotypes through ceRNA mechanisms by directly binding to foreign gene transcripts in HCC, so the role of miR-23b-3p in HCC is critical and has not been fully explored yet. PPIF is a protein-coding gene that encodes a PPIase that catalyzes the cis-trans isomerization of the proline imine peptide bond in oligopeptides and thus may contribute to protein folding (43). PPIase is involved in regulating mitochondrial permeability and cooperates with the TP53 pathway to regulate oxidative stress-induced necrosis (44, 45). In the current study, PPIF negatively regulates ferroptosis in liver cancer cells, which corroborates the function of PPIF to mitochondrial permeability. Moreover, PPIF overexpression can rescue the enhanced ferroptosis caused by DNAJC27-AS1 knockdown or miR-23b-3p mimics; combining the results of the dual luciferase experiments, we have proved the ceRNA mechanism of mutual regulation between PPIF and DNAJC27-AS1 through miR-23b-3p. Above all, we demonstrated the regulatory agency of the DNAJC27-AS1/miR-23b-3p/PPIF axis for ferroptosis at the cellular level in HCC.

The shortcoming of this study is that, firstly, the other ceRNA axes of the constructed ceRNA network were not validated. Secondly, for the ceRNA axis of DNAJC27-AS1/miR-23b-3p/PPIF, only in vitro verification

has been carried out, and no in vivo experiments and clinical experiments have been conducted; these will be studied in the next step. Third, the construction of the ceRNA network depends on the correlation between gene modules and the prediction of website tools; more RNA interaction experiments, like dual-luciferase gene reporter assay, fluorescence in situ hybridization, etc., are required.

There are also three advantages of our study. First, our study constructed the first original ferroptosis-related ceRNA network in HCC through WGCNA analysis and network tools and conducted preliminary verification. Similar ceRNA networks have not been reported in public. Next, the combination of dry and wet research methods made our conclusions more credible. Last but not least, this study is the first to disclose DNAJC27-AS1, miR-23b-3p, and PPIF are closely related to ferroptosis in HCC and reveal the related molecular mechanism.

To sum up, we found the lncRNA, mRNA, and miRNA gene modules closely related to ferroptosis through WGCNA analysis and constructed the ceRNA network accordingly. Then the verification of one axis of the network, DNAJC27-AS1/miR-23b-3p/PPIF, was performed. It was proven to play a considerable role in the ferroptosis of HCC, which also needed much further research. This ceRNA network may provide a reasonable basis for studying ferroptosis and drug resistance in HCC.

Methods

Data collection

The RNA sequencing data of 374 HCC samples and 50 adjacent samples and their associated clinical data were downloaded from the TGCA database (http://portal.gdc.cancer.gov/repository). The autophagy-associated gene set was obtained via Human Autophagy Database (http://www.autophagy.lu/index.html), and the ferroptosis and pytoptosis-associated gene sets were summarized from previously reported studies (46, 47). The three types of gene sets are presented in **Supplementary Table S1**.

Identification of ferroptosis as the target analysis gene sets

The “limma” package was used to analyze the differentially expressed gene sets of the ferroptosis, autophagy, and pytoptosis-associated gene sets. The cut-off value for differential genes was as follows: the absolute value of log fold change ($|\log FC|$) ≥ 1.5, p-value < 0.05. And then used ssGSEA to get the enrichment scores of the ferroptosis-, autophagy-, and pytoptosis-associated gene sets using the “GSVA” R package. Finally, the “survival” R package was applied to compare the survival differences of the ssGSEA scores of the ferroptosis-, autophagy-, and pytoptosis-associated gene sets based on the median cutoff value. The ferroptosis-associated gene set was determined to be aimed for further exploration through survival, univariate, multivariate, and differential analysis.

Analysis of co-expression module construction of HCC

According to the mRNA, lncRNA, and miRNA expression data in LIHC, the co-expression analysis was carried out with the “WGCNA” package. The gradient method was used to test the independence and the average connectivity degree of different modules with different power values (ranging from 1 to 30). The appropriate power value was determined when the degree of independence was 0.8. The correlation between each co-expression module and ferroptosis-related ssGSEA scores was calculated, and the module genes with the strongest correlation were screened for subsequent ceRNA network construction.

Functional enrichment analysis of ferroptosis-related modules

Based on the clusterProfiler R package (48) and GOplot R package (49), candidate genes were analyzed for functional enrichment. Using a statistical algorithm (Fisher's exact test) to find the specific functional items with which the module gene is most associated. The candidate genes here refer to the mRNA modules most associated with ferroptosis. Each item in the results corresponded to a statistical value P-value to indicate significance.

LncRNA-miRNA-mRNA network construction

The lncRNA-miRNA-mRNA network was constructed according to the classical ceRNA network as follows: (a) Interaction prediction of miRNA-mRNAs in the miRmap (50), miRanda (51), miRDB (52), TargetScan (53) and miRTarBase (54), and miRNA-lncRNAs in the miRcode (55), STRBase (56) were identified; (b) Both the lncRNAs and mRNAs were identified by co-expressing negatively with one same miRNA; (c) After intersecting the above-identified lncRNAs, mRNAs, miRNAs, we got the candidates for network construction. The ceRNA regulatory networks were visualized using Cytoscape 3.8.1 software (57).

Cell Lines and Cell Transfection

HepG2 cells, BEL7402 cells, Hep2b, and HuH7 cells were all purchased from ATCC and were cultured in DMEM (Gibco) supplements with 10% fetal bovine serum (Hyclone), 100 U/ml of penicillin (Gibco), and 0.1 mg/ml of streptomycin (Gibco) at 37°C in a humidified atmosphere of 95% O2, 5% CO2.

The overexpression plasmids and siRNAs of DNAJC27-AS1, PPIF, mimic and inhibitor of miR508-3p were provided by GenePharma Co., Ltd. (Shanghai, China). Overexpression plasmid vector is a pEX-3 vector, siRNA sequence information of DNAJC27-AS1 and PPIF are presented in **Supplementary Table S2**. Briefly, cells were transfected with various siRNAs in MEM medium with 90 nM of each siRNA duplex or were transfected with 0.8 ug different plasmids using Lipofectamine 2000 transfection reagent (Thermo Fisher Scientific, Inc.) following the manufacturer's protocol. After transfection for 48 h, cells were harvested for other analyses.

Main reagents and antibodies

Cell Counting Kit-8 (CCK-8) (cat. no. CK04) was purchased from Dojindo Laboratories (Kumamoto, Japan). GSH ELISA kit (cat. no. CEA294Ge) and TP53 antibody (cat. no. PAA928Ra01) were purchased from Cloud-Clone Corp. (Wuhan, China). Cellular ROS Assay Kit (cat. no. ab113851), SLC7A11 antibody

(cat. no. ab175186), GPX4 antibody (cat. no. ab40993), and GAPDH antibody (cat. no. ab8245) were purchased from Abcam (Cambridge, MA, USA). Dual Luciferase Reporter Gene Assay Kit (cat. no. KGAF040) was purchased from KeyGEN BioTECH Co., Ltd (Jiangsu, China). The JC-1 assay kit (cat. no. M8650) was obtained from Solarbio Life Science Co., Ltd (Beijing, China).

Fluorescence Quantitative Real-Time PCR

Quantitative RT-PCR was conducted as per the manufacturer's instructions. In brief, total RNA was isolated using the TRIpure Reagent (RP1001, Bioteke Co., Ltd., Beijing, China). Reverse transcription was performed on 1 μg of RNA at 60°C for 35 min using a BeyoRT II M-MLV (D7160L, Beyotime, Shanghai, China). After reverse transcription, the cDNAs were used for semi-quantitative PCR using 2×Taq PCR MasterMix (PC1150, Solarbio) and SYBR Green (SY1020, Solarbio). Amplification was carried out in the qPCR instrument (LightCycler®480 II, Roche). 25 μl of reaction mixture contained 12.5 μl of SYBRGreen mastermix (SY1020, Solarbio), the appropriate primer concentration, and 1μl of cDNA. The amplification program included the initial denaturation step at 95°C for 10 min, 40 cycles of denaturation at 95°C for 10 s, and annealing and extension at 60°C for 1min. Fluorescence was measured at the end of each extension step. After amplification, melting curves were acquired and used to determine the specificity of the PCR products. $2^{-\triangle\triangle CT}$ method was used in the data process. The sets of specific primers are presented in **Supplementary Table S3**.

Luciferase reporter assay

The bioinformatics tool (Targetscan) was used to predict the miR-23b-3p binding sites of PPIF. Bibiserv was used to predict the miR-23b-3p binding sites of DNAJC27–AS1. According to the above prediction results, the wild-type (wt) binding site sequence was amplified by PCR and then ligated into a dual-luciferase reporter vector, pmirGLO, and site-directed mutation (mut) was made at the possible target site of the target gene. The miR-23b-3p mimics and the above recombinant plasmids were co-transfected into 293T cells in the logarithmic growth phase. The first experiment group is as follows: pmirGLO-wtDNAJC27-AS1+NC mimics, pmirGLO-mutDNAJC27-AS1+NC mimics, pmirGLO-wtDNAJC27-AS1+miR-23b-3p mimics, pmirGLO-mut DNAJC27-AS1+ miR-23b-3p mimics. The second group of experiments is grouped as follows: pmirGLO-PPIF-wtUTR+NC mimics, pmirGLO-PPIF-mutUTR+NC mimics, pmirGLO-PPIF-wtUTR+miR-23b-3p mimics, pmirGLO-PPIF-mutUTR+miR-23b-3p mimics. Forty-eight hours after transfection, the luciferase activity was measured with a multifunction microplate reader (M200Pro, Tecan, Switzerland). The first group of each experiment was set as the control.

Western blotting

HepG2 and BEL7402 cells were harvested and washed with PBS after drug treatment or genetic manipulation. Total cellular protein was isolated using the protein extraction buffer (containing 150 mM NaCl, 10 mM Tris (pH 7.2), 5 mM EDTA, 0.1% Triton X-100, 5% glycerol, and 2% SDS). Equal amounts of proteins (50 μg/lane) were fractionated using 10% SDS–PAGE and transferred to PVDF membranes. The membranes were incubated with primary antibodies. After washing with PBS, the membranes were

incubated with corresponding peroxidase-conjugated goat anti-mouse or anti-rabbit secondary antibody, followed by enhanced chemiluminescence staining through the enhanced chemiluminescence system. GAPDH was used to normalize protein loading.

ROS and mitochondrial membrane potential detection by flow cytometry

2'-7'-dichlorodihydrofluorescein-diacetate (DCFHDA) penetrates cells and becomes hydrolyzed to non-fluorescent dichlorodihydrofluorescein (DCFH). DCFH reacts with ROS to form the highly fluorescent dichlorofluorescein (DCF), which flow cytometry can measure. Briefly, HepG2 and BEL7402 cells were treated and collected at least 1.5×10^4 per assayed condition. Staining cells in culture media with 20 μM DCFHDA and incubating for 30 minutes at 37°C. Washing cells with 1× Buffer after incubation. Then DCF fluorescence distribution of at least 10000 cells was detected by a Novocyte Flow Cytometer (ACEA, Bioscience, USA). Establish forward and side scatter gates to exclude debris and cellular aggregates from the analysis. DCF is excited by the 488 nm laser and detected at 535 nm.

The JC-1 kit determined the mitochondrial membrane potential. The working solution was prepared as instruction. Firstly, 1ml JC-1 working solution was used to suspend the cells and incubated at 5% CO2 and 37 ℃ for 20 min. After washing twice with incubation buffer, the cells were resuspended with 1 ml incubation buffer; then, flow cytometry analysis was conducted. Excitation was set at 488 nm.

Cell viability and GSH assay

The cells were seeded into 96-well microtiter plates at 3,000 cells/well density and allowed to adhere for 12 h. Cells were then treated differently according to the grouping, then exposed to CCK-8 (10 μl/well) for 2 h at 37°C. Absorbance was measured at 450 nm on a Tecan Sunrise microplate reader (Tecan Group AG, Männedorf, Switzerland). For GSH detection, cells (1×106 cells/well) were seeded in 6-well plates and then treated differently. Following treatment, cells were harvested by centrifugation and lysed on ice for 30 min using lysis buffer (50 mmol Tris-HCl, 1.0 mmol/l EDTA, 150 mmol/l NaCl, and 0.1% SDS) and centrifuged once more at 5,000×g for 10 min at 4°C. The supernatant was used for the GSH assays as per the manufacturer's instructions. Briefly, add 50μL samples to each well. And then add 50μL prepared Detection Reagent A immediately. Incubate for 1 hour at 37℃. Add 100μL prepared Detection Reagent B after aspiration and wash. Incubate for 30 minutes at 37℃. Add 90μL Substrate Solution after aspiration and wash. Incubate for 15 minutes at 37℃. Add 50μL Stop Solution and read at 450 nm immediately.

Statistical analysis

Data are presented as the mean±standard deviation (SD) of at least three independent experiments. The Student's t-test for comparison of two groups or one-way analysis of variance (ANOVA) for comparison of multiple groups followed by Tukey's multiple comparison test. For multiple testing, a Bonferroni post hoc test of P-values was made. Statistical analysis was performed using GraphPad Prism 8 (GraphPad, Inc., San Diego, CA, USA). P value less than 0.05 means statistically significant.

Declarations

Acknowledgments

Not applicable.

Author contributions

TG and KH participated in the design of this study, WC and JS performed the analysis, ZY drafted the manuscript. MX collected important background information. YC participated in the design and helped to draft the manuscript. All authors read and approved the final manuscript.

Competing interests

The authors declare no competing interest

Data availability

The data supporting the finding of this study are available from the corresponding author upon reasonable request.

Ethics declarations

Not applicable.

Funding

The authors received no specific funding for this work.

References

1. Yang W, Ma Y, Liu Y, Smith-Warner SA, Simon TG, Chong DQ, et al. Association of intake of whole grains and dietary fiber with risk of hepatocellular carcinoma in US adults. *JAMA Oncol* . **5**, 879-886 (2019).
2. Shin S, Wangensteen KJ, Teta-Bissett M, Wang YJ, Mosleh-Shirazi E, Buza EL, et al. Genetic lineage tracing analysis of the cell of origin of hepatotoxin-induced liver tumors in mice. *Hepatology.* **64**, 1163-1177 (2016).
3. Kwan SY, Sheel A, Song CQ, Zhang XO, Jiang T, Dang H, et al. Depletion of TRRAP induces p53-independent senescence in liver cancer by down-regulating mitotic genes. *Hepatology*. **71**, 275-290 (2020).
4. Zhu S, Zhang Q, Sun X, Zeh HJ, Lotze MT, Kang R, et al. HSPA5 regulates ferroptotic cell death in cancer cells. *Cancer Res*. **77**, 2064-2077 (2017).
5. Koren E, Fuchs Y. Modes of regulated cell death in cancer. *Cancer Discov*. **11**, 245-265 (2021).

6. Vanden Berghe T, Linkermann A, Jouan-Lanhouet S, Walczak H, Vandenabeele P. Regulated necrosis: the expanding network of non-apoptotic cell death pathways. *Nat Rev Mol Cell Biol*. **15**, 135-147 (2014).
7. Dixon SJ, Lemberg KM, Lamprecht MR, Skouta R, Zaitsev EM, Gleason CE, et al. Ferroptosis: an iron-dependent form of nonapoptotic cell death. *Cell*. **149**, 1060-1072 (2012).
8. Yagoda N, von Rechenberg M, Zaganjor E, Bauer AJ, Yang WS, Fridman DJ, et al. RAS-RAF-MEK-dependent oxidative cell death involving voltage-dependent anion channels. *Nature*. **447**, 864-868 (2007).
9. Chen PH, Wu J, Ding CC, Lin CC, Pan S, Bossa N, et al. Kinome screen of ferroptosis reveals a novel role of ATM in regulating iron metabolism. *Cell Death Differ*. **27**, 1008-1022 (2020).
10. Yee PP, Wei Y, Kim SY, Lu T, Chih SY, Lawson C, et al. Neutrophil-induced ferroptosis promotes tumor necrosis in glioblastoma progression. *Nat Commun*. **11**, 5424; 10.1038/s41467-020-19193-y (2020).
11. Chu B, Kon N, Chen D, Li T, Liu T, Jiang L, et al. ALOX12 is required for p53-mediated tumour suppression through a distinct ferroptosis pathway. *Nat Cell Biol*. **21**, 579-591 (2019).
12. Capelletti MM, Manceau H, Puy H, Peoc'h K. Ferroptosis in Liver Diseases: An Overview. *Int J Mol Sci*. **21(14)**, 4908; 10.3390/ijms21144908 (2020).
13. Du J, Wan Z, Wang C, Lu F, Wei M, Wang D, et al. Designer exosomes for targeted and efficient ferroptosis induction in cancer via chemo-photodynamic therapy. *Theranostics*. **11**, 8185-8196 (2021).
14. Sun X, Niu X, Chen R, He W, Chen D, Kang R, et al. Metallothionein-1G facilitates sorafenib resistance through inhibition of ferroptosis. *Hepatology*. **64**, 488-500 (2016).
15. Gao R, Kalathur RKR, Coto-Llerena M, Ercan C, Buechel D, Shuang S, et al. YAP/TAZ and ATF4 drive resistance to sorafenib in hepatocellular carcinoma by preventing ferroptosis. *EMBO Mol Med*. **13**, e14351; 10.15252/emmm.202114351 (2021).
16. Shi Y, Liu JB, Deng J, Zou DZ, Wu JJ, Cao YH, et al. The role of ceRNA-mediated diagnosis and therapy in hepatocellular carcinoma. *Hereditas*. **158**, 44; 10.1186/s41065-021-00208-7 (2021).
17. Wang H, Huo X, Yang XR, He J, Cheng L, Wang N, et al. STAT3-mediated upregulation of lncRNA HOXD-AS1 as a ceRNA facilitates liver cancer metastasis by regulating SOX4. *Mol Cancer*. **16**, 136; 10.1186/s12943-017-0680-1 (2017).
18. Chen J, Yu Y, Li H, Hu Q, Chen X, He Y, et al. Long non-coding RNA PVT1 promotes tumor progression by regulating the miR-143/HK2 axis in gallbladder cancer. *Mol Cancer*. **18**, 33; 10.1186/s12943-019-0947-9 (2019).
19. Weng W, Zhang Z, Huang W, Xu X, Wu B, Ye T, et al. Identification of a competing endogenous RNA network associated with prognosis of pancreatic adenocarcinoma. *Cancer Cell Int*. **20**, 231; 10.1186/s12935-020-01243-6 (2020).
20. Xu M, Chen X, Lin K, Zeng K, Liu X, Xu X, et al. lncRNA SNHG6 regulates EZH2 expression by sponging miR-26a/b and miR-214 in colorectal cancer. *J Hematol Oncol*. **12**, 3; 10.1186/s13045-018-0690-5 (2019).

21. Qi W, Li Z, Xia L, Dai J, Zhang Q, Wu C, et al. LncRNA GABPB1-AS1 and GABPB1 regulate oxidative stress during erastin-induced ferroptosis in HepG2 hepatocellular carcinoma cells. *Sci Rep*. **9**, 16185; 10.1038/s41598-019-52837-8 (2019).
22. Zhang Y, Luo M, Cui X, O'Connell D, Yang Y. Long noncoding RNA NEAT1 promotes ferroptosis by modulating the miR-362-3p/MIOX axis as a ceRNA. *Cell Death Differ*. 10.1038/s41418-022-00970-9 (2022).
23. Mao C, Wang X, Liu Y, Wang M, Yan B, Jiang Y, et al. A G3BP1-Interacting lncRNA promotes ferroptosis and apoptosis in cancer via nuclear sequestration of p53. *Cancer Res*. **78**, 3484-3496 (2018).
24. Ye Y, Dai Q, Qi H. A novel defined pyroptosis-related gene signature for predicting the prognosis of ovarian cancer. *Cell Death Discov*. **7**, 71; 10.1038/s41420-021-00451-x (2021).
25. Wan RJ, Peng W, Xia QX, Zhou HH, Mao XY. Ferroptosis-related gene signature predicts prognosis and immunotherapy in glioma. *CNS Neurosci Ther*. **27**, 973-986 (2021).
26. Yu G, Wang LG, Han Y, He QY. clusterProfiler: an R package for comparing biological themes among gene clusters. *OMICS*. **16**, 284-287 (2012).
27. Walter W, Sanchez-Cabo F, Ricote M. GOplot: an R package for visually combining expression data with functional analysis. Bioinformatics. **31**, 2912-2914 (2015).
28. Vejnar CE, Blum M, Zdobnov EM. MiRmap web: comprehensive microRNA target prediction online. *Nucleic Acids Res*. **41**, W165-168 (2013).
29. Miranda KC, Huynh T, Tay Y, Ang YS, Tam WL, Thomson AM, et al. A pattern-based method for the identification of MicroRNA binding sites and their corresponding heteroduplexes. *Cell*. **126**, 1203-1217 (2006).
30. Wong N, Wang X. MiRDB: an online resource for microRNA target prediction and functional annotations. *Nucleic Acids Res*. **43**, D146-152 (2015).
31. Nielsen CB, Shomron N, Sandberg R, Hornstein E, Kitzman J, Burge CB. Determinants of targeting by endogenous and exogenous microRNAs and siRNAs. *RNA*. **13**, 1894-1910 (2007).
32. Huang HY, Lin YC, Li J, Huang KY, Shrestha S, Hong HC, et al. MiRTarBase 2020: updates to the experimentally validated microRNA-target interaction database. *Nucleic Acids Res*. **48**, D148-D154 (2020).
33. Jeggari A, Marks DS, Larsson E. MiRcode: a map of putative microRNA target sites in the long non-coding transcriptome. *Bioinformatics*. **28**, 2062-2063 (2012).
34. Li JH, Liu S, Zhou H, Qu LH, Yang JH. StarBase v2.0: decoding miRNA-ceRNA, miRNA-ncRNA and protein-RNA interaction networks from large-scale CLIP-Seq data. *Nucleic Acids Res*. **42**, D92-97 (2014).
35. Shannon P, Markiel A, Ozier O, Baliga NS, Wang JT, Ramage D, et al. Cytoscape: a software environment for integrated models of biomolecular interaction networks. *Genome Res*. **13**, 2498-2504 (2003).

36. Cancer Genome Atlas Research Network. Comprehensive and integrative genomic characterization of hepatocellular carcinoma. *Cell*. 169, 1327-1341; 10.1016/j.cell.2017.05.046 (2017).
37. Nie J, Lin B, Zhou M, Wu L, Zheng T. Role of ferroptosis in hepatocellular carcinoma. *J Cancer Res Clin Oncol*. **144**, 2329-2337 (2018).
38. Louandre C, Ezzoukhry Z, Godin C, Barbare JC, Maziere JC, Chauffert B, et al. Iron-dependent cell death of hepatocellular carcinoma cells exposed to sorafenib. *Int J Cancer*. **133**, 1732-1742 (2013).
39. Jennis M, Kung CP, Basu S, Budina-Kolomets A, Leu JI, Khaku S, et al. An African-specific polymorphism in the TP53 gene impairs p53 tumor suppressor function in a mouse model. *Genes Dev*. **30**, 918-930 (2016).
40. Louandre C, Marcq I, Bouhlal H, Lachaier E, Godin C, Saidak Z, et al. The retinoblastoma (Rb) protein regulates ferroptosis induced by sorafenib in human hepatocellular carcinoma cells. *Cancer Lett*. **356**, 971-977 (2015).
41. Yu J, Wang JQ. Research mechanisms of and pharmaceutical treatments for ferroptosis in liver diseases. *Biochimie*. **180**, 149-157 (2021).
42. Salmena L, Poliseno L, Tay Y, Kats L, Pandolfi PP. A ceRNA hypothesis: the Rosetta Stone of a hidden RNA language? *Cell*. **146**, 353-358 (2011).
43. Chen L, Yao H, Wang K, Liu X. Long non-coding RNA MALAT1 regulates ZEB1 expression by sponging miR-143-3p and promotes hepatocellular carcinoma progression. *J Cell Biochem*. **118**, 36-4843 (2017).
44. Hou Z, Xu X, Zhou L, Fu X, Tao S, Zhou J, et al. The long non-coding RNA MALAT1 promotes the migration and invasion of hepatocellular carcinoma by sponging miR-204 and releasing SIRT1. *Tumour Biol*. **39**, 7; 10.1177/1010428317718135 (2017).
45. Pan Y, Tong S, Cui R, Fan J, Liu C, Lin Y, et al. Long non-coding MALAT1 functions as a competing endogenous RNA to regulate vimentin expression by sponging miR-30a-5p in hepatocellular carcinoma. *Cell Physiol Biochem*. **50**, 108-120 (2018).
46. Wang J, Liu X, Wu H, Ni P, Gu Z, Qiao Y, et al. CREB up-regulates long non-coding RNA HULC expression through interaction with microRNA-372 in liver cancer. *Nucleic Acids Res*. **38**, 5366-5383 (2010).
47. Li SP, Xu HX, Yu Y, He JD, Wang Z, Xu YJ, et al. LncRNA HULC enhances epithelial-mesenchymal transition to promote tumorigenesis and metastasis of hepatocellular carcinoma via the miR-200a-3p/ZEB1 signaling pathway. *Oncotarget*. **7**, 42431-42446 (2016).
48. Xiong H, Ni Z, He J, Jiang S, Li X, He J, et al. LncRNA HULC triggers autophagy via stabilizing Sirt1 and attenuates the chemosensitivity of HCC cells. *Oncogene*. **36**, 3528-3540 (2017).
49. Fei X, Hu C, Wang X, Lu C, Chen H, Sun B, et al. Construction of a ferroptosis-related long non-coding RNA prognostic signature and competing endogenous RNA network in lung adenocarcinoma. *Front Cell Dev Biol*.. **9**,751490; 10.3389/fcell.2021.751490 (2021).
50. Zhou M, Lu B, Tan W, Fu M. Identification of lncRNA-miRNA-mRNA regulatory network associated with primary open angle glaucoma. *BMC Ophthalmol*. **20**, 104; 10.1186/s12886-020-01365-5 (2020).

51. Hayashi M, Yamada S, Kurimoto K, Tanabe H, Hirabayashi S, Sonohara F, et al. miR-23b-3p plays an oncogenic role in hepatocellular carcinoma. *Ann Surg Oncol*. **28**, 3416-3426 (2021).
52. Manganelli M, Grossi I, Ferracin M, Guerriero P, Negrini M, Ghidini M, et al. Longitudinal circulating levels of miR-23b-3p, miR-126-3p and lncRNA GAS5 in HCC patients treated with sorafenib. *Biomedicines*. **9**, 813; 10.3390/biomedicines9070813 (2021).
53. Jing Z, Ye X, Ma X, Hu X, Yang W, Shi J, et al. SNGH16 regulates cell autophagy to promote sorafenib resistance through suppressing miR-23b-3p via sponging EGR1 in hepatocellular carcinoma. *Cancer Med*. **9**, 4324-4338 (2020).
54. Yang T, He X, Chen A, Tan K, Du X. LncRNA HOTAIR contributes to the malignancy of hepatocellular carcinoma by enhancing epithelial-mesenchymal transition via sponging miR-23b-3p from ZEB1. *Gene*. **670**, 114-122 (2018).
55. Davis TL, Walker JR, Campagna-Slater V, Finerty PJ, Paramanathan R, Bernstein G, et al. Structural and biochemical characterization of the human cyclophilin family of peptidyl-prolyl isomerases. *PLoS Biol*. **8**, 7; 10.1371/journal.pbio.1000439 (2010).
56. Shanmughapriya S, Rajan S, Hoffman NE, Higgins AM, Tomar D, Nemani N, et al. SPG7 is an essential and conserved component of the mitochondrial permeability transition pore. *Mol Cell*. **60**, 47-62 (2015).
57. Vaseva AV, Marchenko ND, Ji K, Tsirka SE, Holzmann S, Moll UM. p53 opens the mitochondrial permeability transition pore to trigger necrosis. *Cell*. **149**, 1536-1548 (2012).

Figures

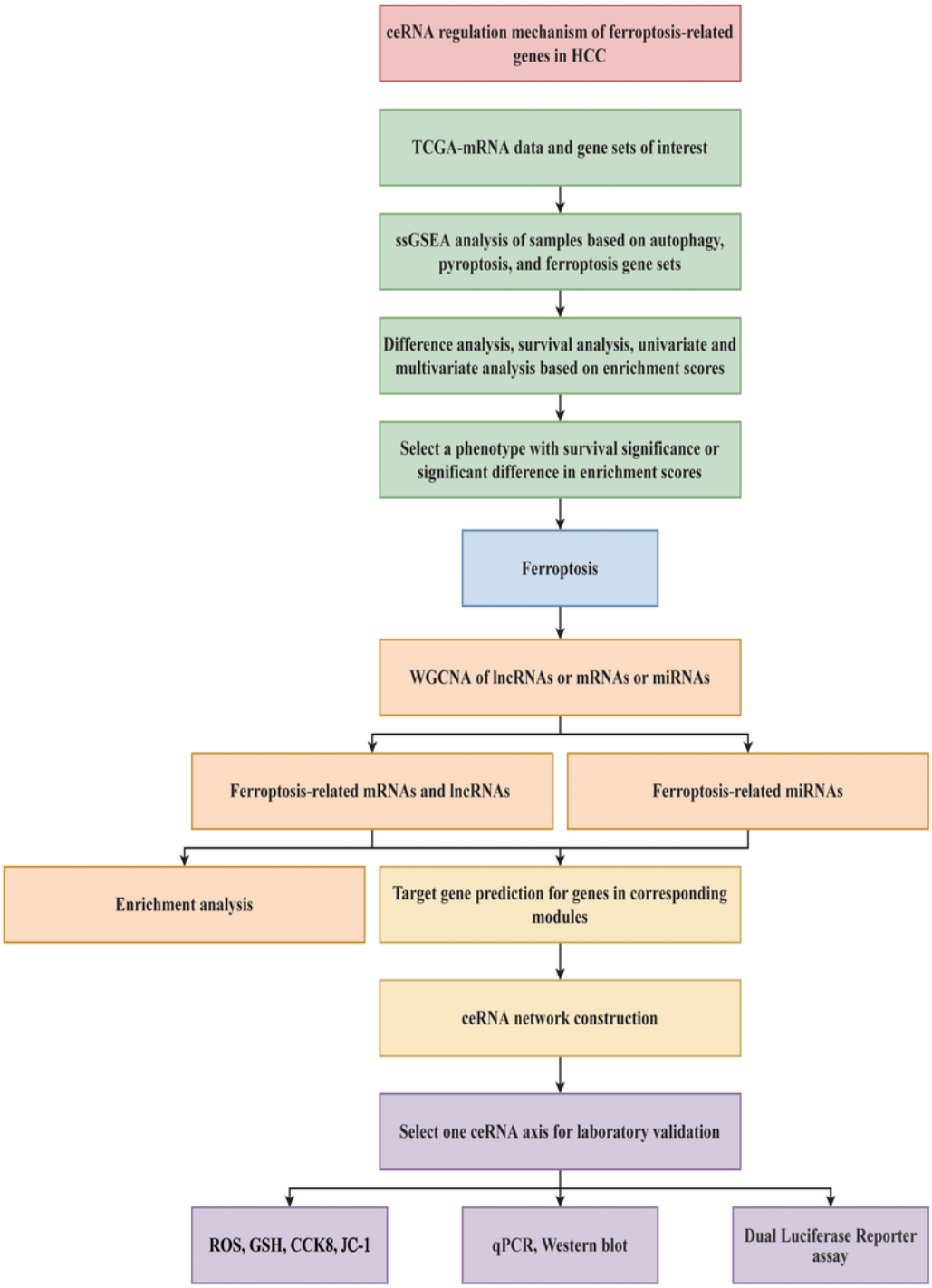

Figure 1

Flow chart in this study.

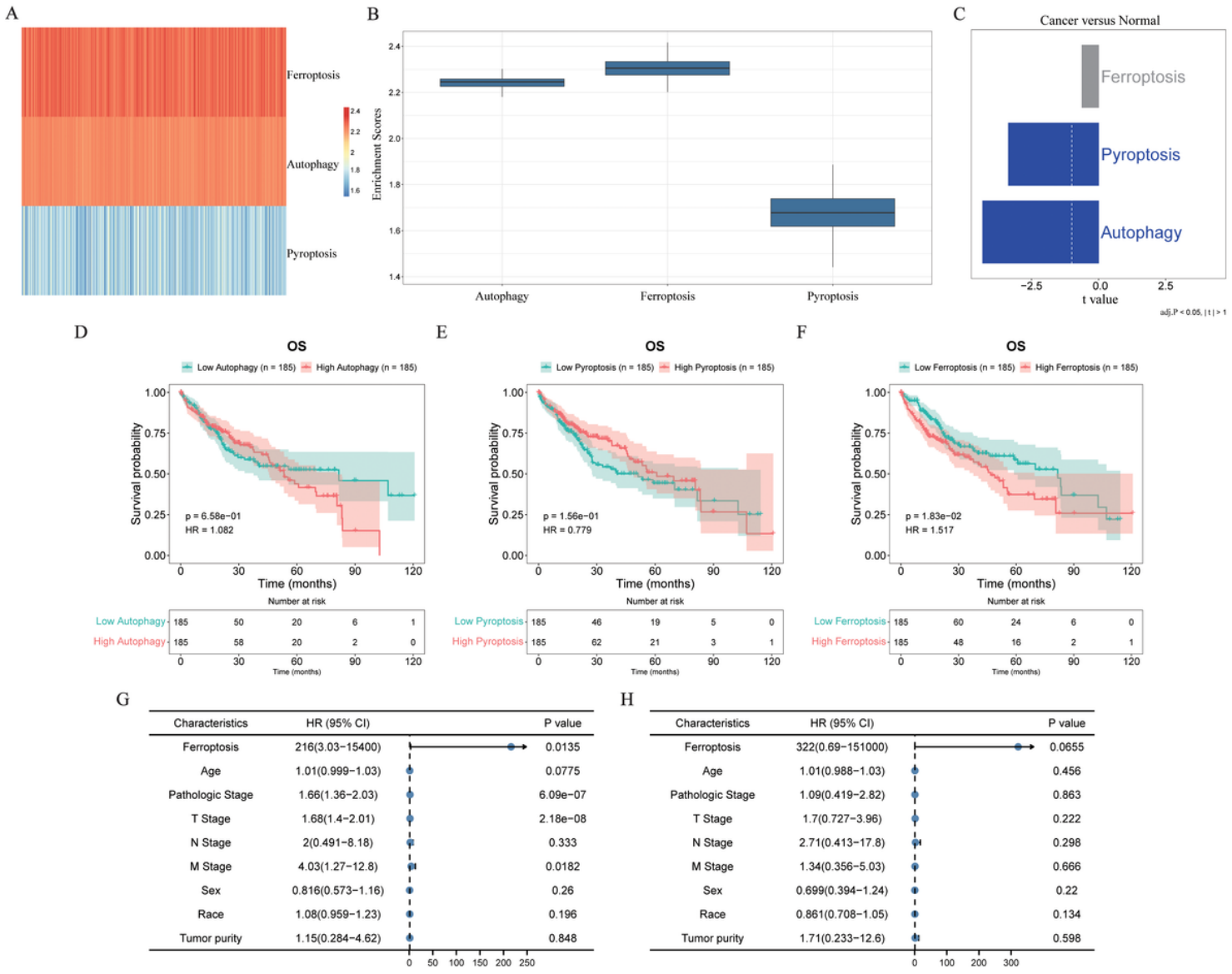

Figure 2

Differential analysis and survival analysis of ssGSEA scores related to ferroptosis, autophagy, and pyroptosis. (**A**) Heatmap of ssGSEA scores for the three phenotypes. (**B**) Boxplots of ssGSEA scores for the three phenotypes. (**C**) Differential analysis of ssGSEA scores for the three phenotypes. (**D**) Kaplan-Meier survival analysis of ssGSEA scores for autophagy. (**E**) Kaplan-Meier survival analysis of ssGSEA scores for pyroptosis. (**F**) Kaplan-Meier survival analysis of ssGSEA scores for ferroptosis. (**G**) Univariate analysis of ssGSEA scores for ferroptosis. (**H**) Multivariate analysis of ssGSEA scores for ferroptosis.

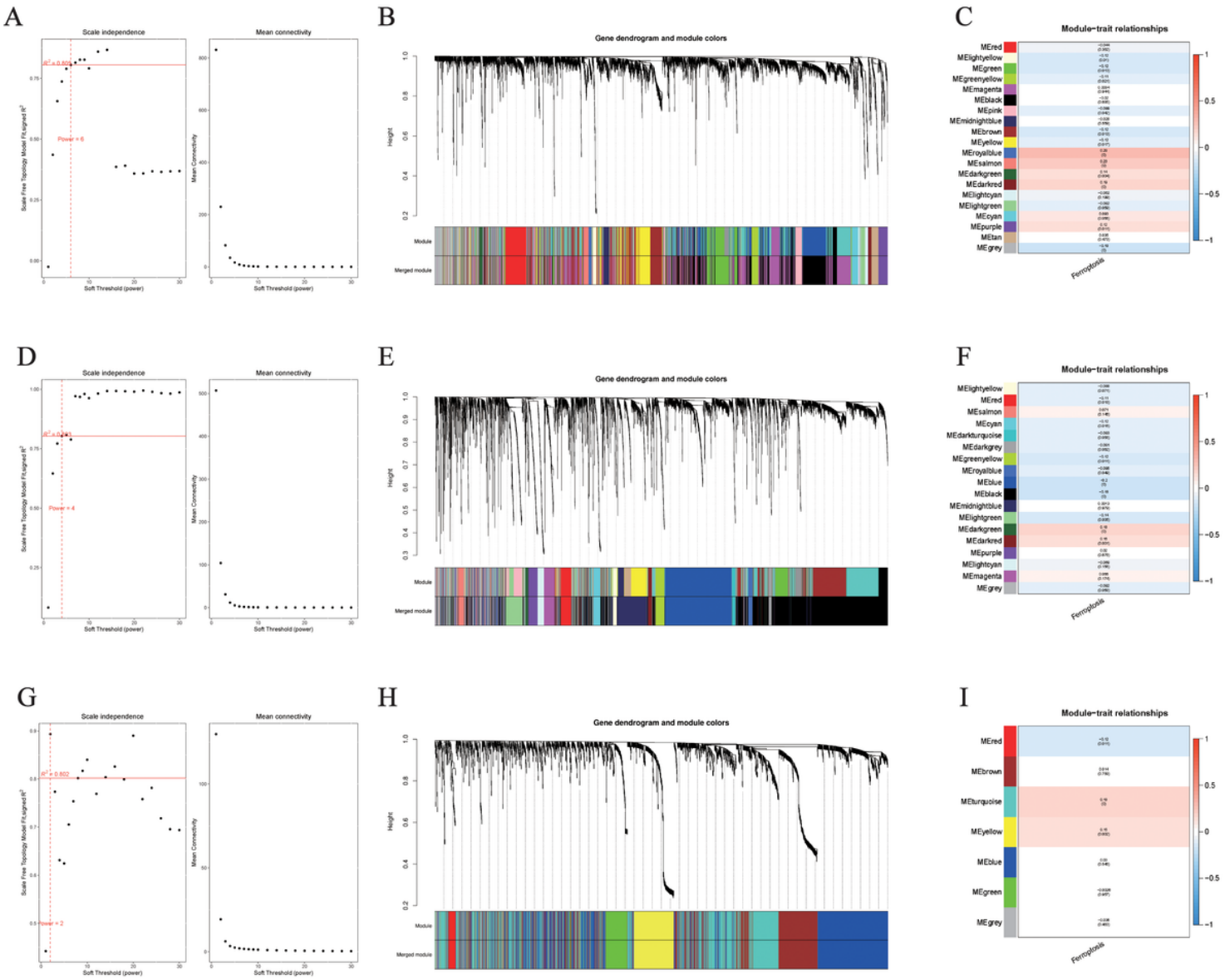

Figure 3

Analysis of network topology for various soft-thresholding powers, clustering dendrograms for the three types of genes, and heatmap for the relationships of the module trait. (**A**) In the WGCNA analysis of mRNA, the soft-thresholding power was set to 6. (**B**) A total of 20 mRNA co-expression modules were constructed and shown in different colors. (**C**) Each color corresponds to a module eigengene of mRNA; each cell contains the corresponding ferroptosis correlation and p-value. (**D-F**) In the WGCNA analysis of lncRNA, the soft-thresholding power was set to 4, a total of 18 mRNA co-expression modules were constructed, and the corresponding correlation between modules and ferroptosis was shown. (**G-I**) The WGCNA analysis of miRNA.

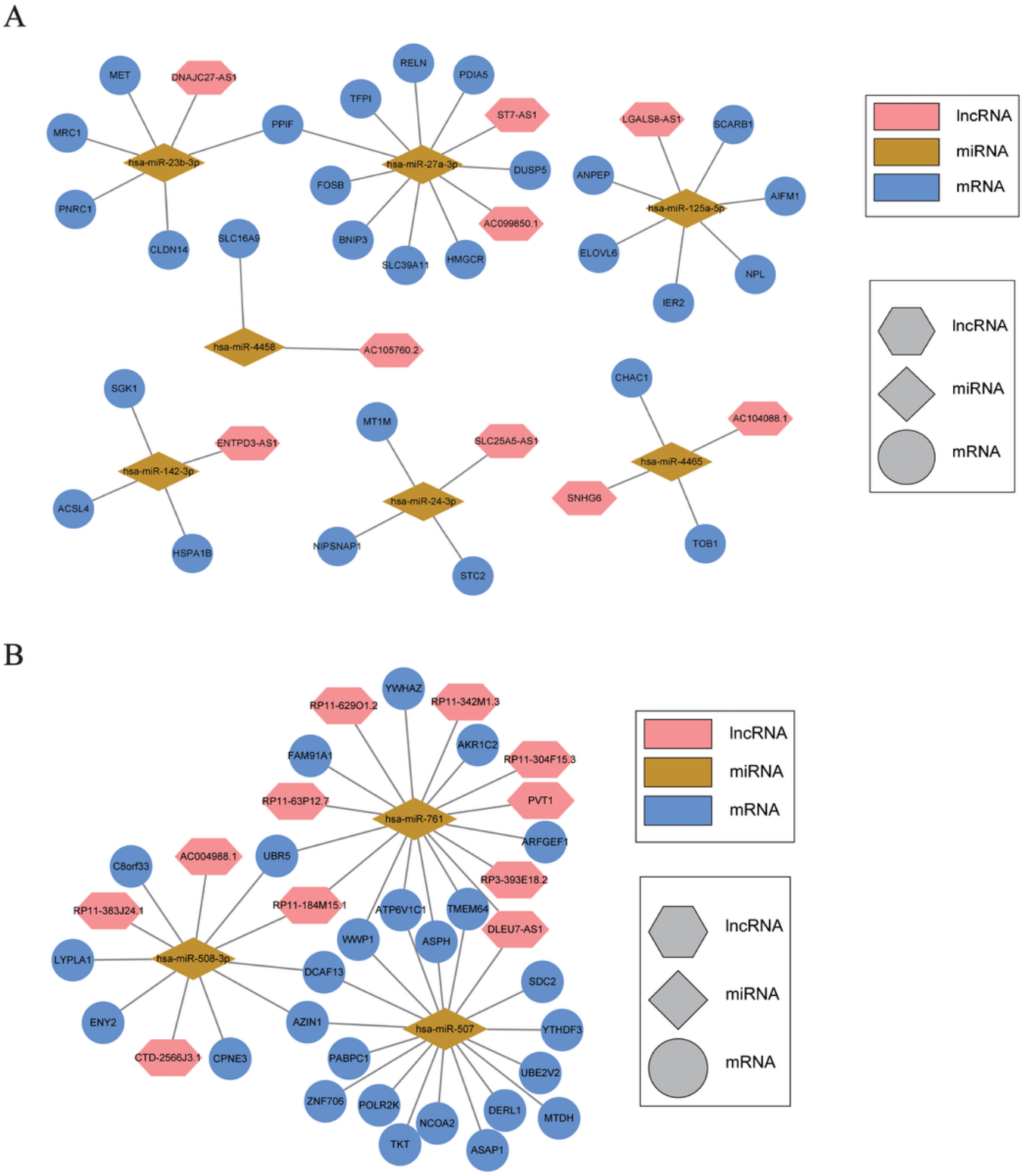

Figure 4

The ceRNA network construction. (**A**) The ceRNA network consists of the negative ferroptosis-related lncRNAs and mRNAs, and the positive ferroptosis-related miRNAs. (**B**) The ceRNA network consists of the positive ferroptosis-related lncRNAs and mRNAs, and the negative ferroptosis-related miRNAs.

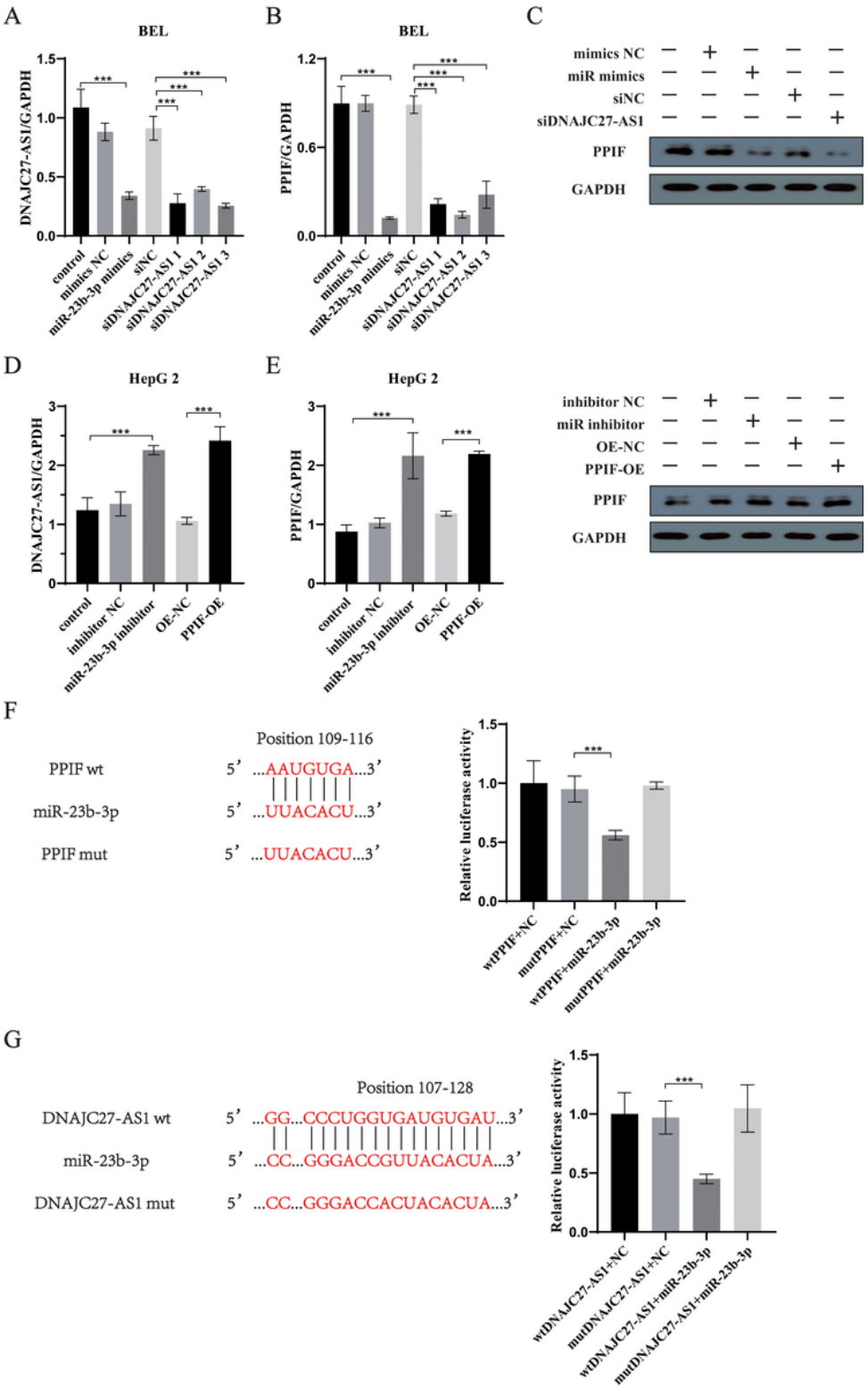

Figure 5

DNAJC27-AS1 and PPIF regulate each other's expression through direct interaction with miR-23b-3p. (**A**) miR-23b-3p mimics can inhibit the transcription level of DNAJC27-AS1 and the efficiency verification of siDNAJC27-AS1. (**B-C**) Both miR-23b-3p mimics, and siDNAJC27-AS1 can inhibit the transcriptional level and the expression of PPIF. (**D**) The miR-23b-3p inhibitor can elevate the transcriptional level of PPIF and the efficiency verification of PPIF overexpression plasmid. (**E-F**) Both miR-23b-3p inhibitor and PPIF

overexpression can elevate the transcriptional level and the expression of DNAJC27-AS1. (**G**) DNAJC27-AS1 and miR-23b-3p have direct interaction at positions 107 to 128 of DNAJC27-AS1. (**H**) PPIF and miR-23b-3p have direct interaction at positions 109 to 116 of PPIF. OE refers to overexpression. BEL refers to the BEL7402 cell line. NC refers to the negative control. Wt refers to wild type. Mut refers to mutant. **p < 0.01, ***p < 0.001.

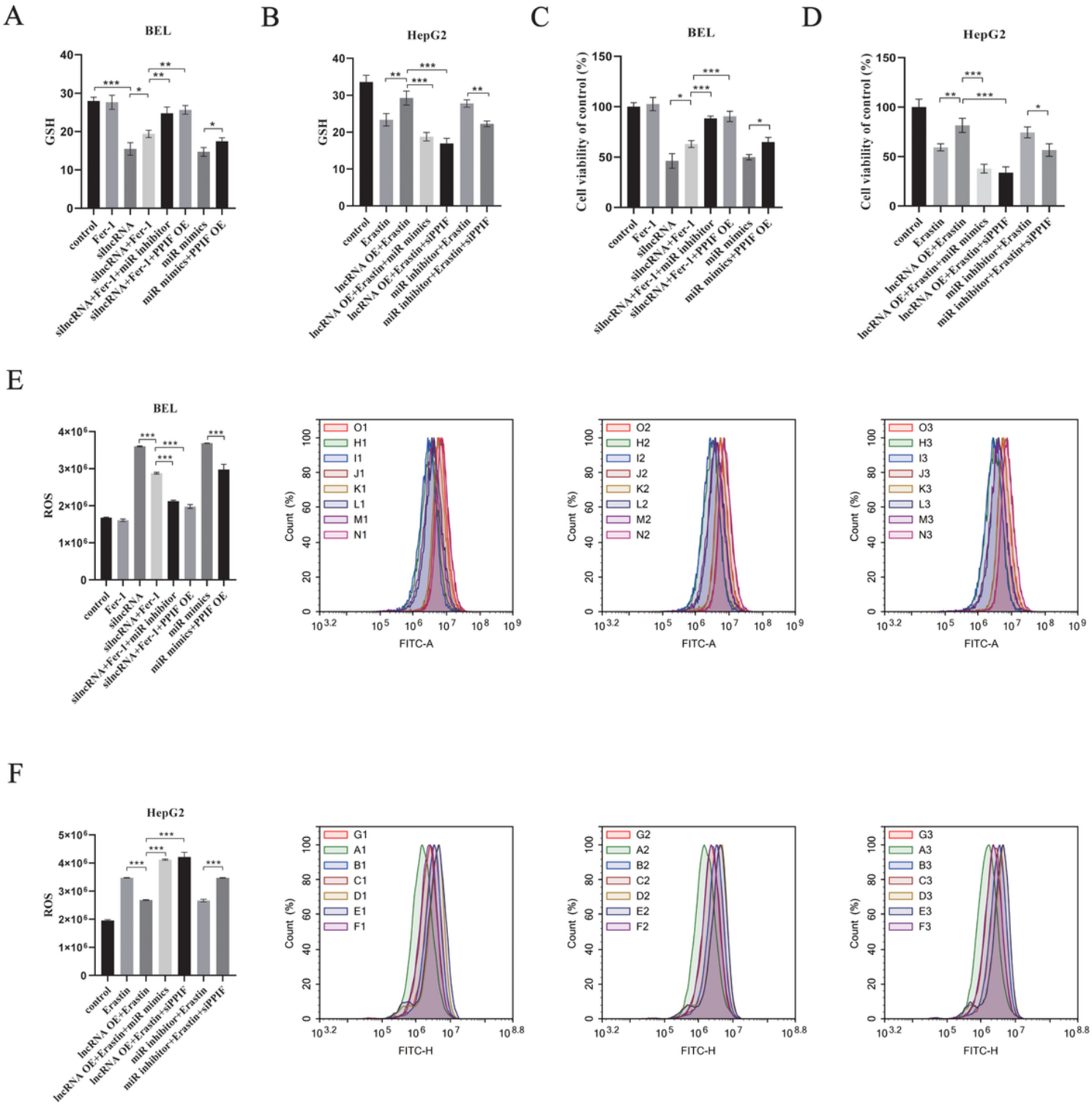

Figure 6

DNAJC27-AS1/miR-23b-3p/PPIF axis regulates ferroptosis in HCC cells. (**A**) Detection of GSH content in BEL cells. (**B**) Detection of GSH content in HepG2 cells. (**C**) Cell viability assays in BEL cells. (**D**) Cell viability assays in HepG2 cells. (**E**) siDNAJC27-AS1 and miR-23b-3p mimic promote ROS production in BEL cells, while miR-23b-3p inhibitor and PPIF overexpression reduce ROS production. (**F**) DNAJC27-AS1 overexpression reduces ROS production in HepG2 cells, while siPPIF promotes ROS production. LncRNA refers to DNAJC27-AS1. MiR refers to miR23b-3p. BEL refers to the BEL7402 cell line. OE refers to overexpression. *p<0.05, **p<0.01, ***p<0.001.

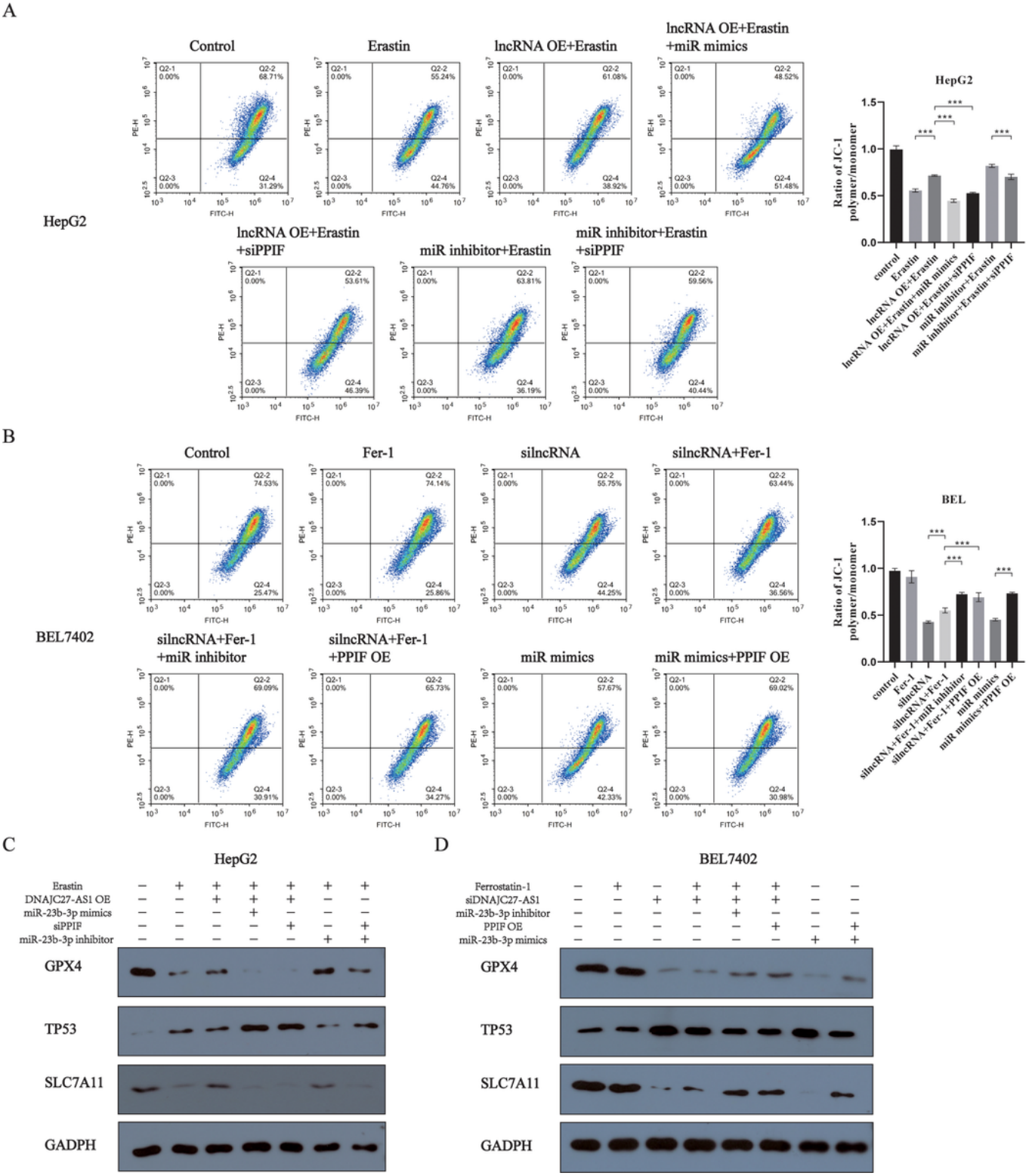

Figure 7

DNAJC27-AS1/miR-23b-3p/PPIF axis regulates ferroptosis through a ceRNA mechanism. (**A-B**) Mitochondrial membrane potential detection of HepG2 cells in each group. (**C-D**) Immunoblotting of ferroptosis markers GPX4, TP53, and SLC7A11 in each group of HCC cells. BEL refers to the BEL7402 cell line. OE refers to overexpression. ***p<0.001.

Supplementary Files

This is a list of supplementary files associated with this preprint. Click to download.

- SupplementaryMaterial1.xls
- SupplementaryMaterial2.xls
- SupplementaryMaterial3.xls
- SupplementaryMaterial4.xls
- TableS1.docx
- TableS2.docx
- TableS3.docx
- FigureS1.tif
- FigureS2.tif
- FigureS3.tif
- FigureS4.tif